Soil Dynamics and Earthquake Engineering 88 (2016) 427–438

Contents lists available at ScienceDirect

Soil Dynamics and Earthquake Engineering

journal homepage: www.elsevier.com/locate/soildyn

A centrifuge study of the influence of site response, relative stiffness, and kinematic constraints on the seismic performance of buried reservoir structures

A. Hushmand [a], S. Dashti [a,*], C. Davis [b], J.S. McCartney [c], B. Hushmand [d]

[a] University of Colorado Boulder, Civil, Env. and Arch. Engineering, Boulder, CO, United States
[b] Los Angeles Department of Water and Power, Los Angeles, CA, United States
[c] Univ. of California at San Diego, Department of Structural Engineering, San Diego, CA, United States
[d] Hushmand Associates, Inc., Irvine, CA, United States

ARTICLE INFO

Article history:
Received 7 February 2016
Received in revised form
1 May 2016
Accepted 20 June 2016

Keywords:
Underground reservoir structures
Seismic soil-structure interaction
Centrifuge modeling
Seismic earth pressures
Site response
Sinusoidal and earthquake motions

ABSTRACT

The seismic performance of underground reservoir structures depends on the properties of the structure, soil, and ground motion as well as the kinematic constraints imposed on the structure. A series of four centrifuge experiments were performed to evaluate the influence of site response, structural stiffness, base fixity, and excitation frequency on the performance of relatively stiff reservoir structures buried in dry, medium-dense sand. The magnitude of seismic thrust increased and the distribution of seismic earth pressures changed from approximately triangular to parabolic with increasing structural stiffness. Heavier and stiffer structures also experienced increased rocking and reduced flexural deflection. Fixing the base of the structure amplified the magnitude of acceleration, seismic earth pressure, and bending strain compared to tests where the structure was free to translate laterally, settle, or rotate atop a soil layer. The frequency content of transient tilt, acceleration, dynamic thrust, and bending strain measured on the structure was strongly influenced by that of the base motion and site response, but was unaffected by the fundamental frequency of the buried structure ($f_{structure}$). None of the available simplified procedures could capture the distribution and magnitude of seismic earth pressures experienced by this class of underground structures. The insight from this experimental study is aimed to help validate analytical and numerical methods used in the seismic design of reservoir structures.

1. Introduction

The seismic response of stiff-unyielding underground structures with minimum to no soil overburden is a fairly new topic at the interface between geotechnical and structural engineering. Buried structures can be classified as stiff-unyielding when they do not deform or rotate enough during seismic events to create active (yielding) conditions in the backfill soil due to the kinematic constraints at their roof or base, while they are not completely rigid and deform according to their stiffness. The majority of previous analytical, numerical, and physical model studies on the seismic response of buried structures focused on either yielding or rigid-unyielding underground structures (e.g., [1,5,6,16–19,22,23,25,27]). However, a number of important buried structures such as nuclear facilities, bunkers, culverts, and water reservoirs can be categorized as stiff-unyielding. The focus of this paper is on the seismic response of this type of structure (flexibility ratios ranging from approximately 0.1 to 2), particularly focusing on the buried water reservoirs being built by the Los Angeles Department of Water and Power (LADWP).

The seismic forces and deformations experienced by stiff-unyielding underground structures are not well understood. Soil-structure interaction near these structures is governed by the dynamic properties of the structure and backfill soil as well as the imposed kinematic constraints on the structure and the intensity, duration, and frequency content of the earthquake motion [2,11,12]. The available simplified procedures for buried structures introduced by Mononobe-Okabe [17,18], Seed-Whitman [22], or Wood [27] do not consider all of these effects. Although advanced numerical tools can take these effects into account, they may lead to complexities that require validation against the results from field observations or physical model studies.

Several of the previous experimental studies primarily focused on either yielding retaining structures [1,16,23] or flexible tunnels with large overburden (e.g., [3,24]). However, the seismic response of these structures is different from the stiff-unyielding structures

* Corresponding author.
E-mail address: shideh.dashti@colorado.edu (S. Dashti).

http://dx.doi.org/10.1016/j.soildyn.2016.06.011
0267-7261/

with shallow or no overburden considered in this study. In response to this shortcoming, a series of dynamic centrifuge tests were recently conducted at the University of Colorado Boulder to evaluate the seismic performance of buried reservoirs with varying structural rigidity, soil cover, backfill soil type, backfill geometry, base fixity, and container boundary conditions. Hushmand et al. [11,12] summarized the insight obtained from these experiments regarding the influences of structural stiffness and the type and geometry of the backfill soil during earthquake loading. These experiments showed that stiff-unyielding buried structures could experience notable dynamic earth pressures. However, none of the available simplified procedures for buried structures was able to sufficiently capture the distribution and magnitude of seismic earth pressures or deformations experienced by the class of stiff-unyielding structures under the loading scenarios often used in their design. Further, the critical role of site response was displayed on the forces measured on the buried structures. Yet, the interacting influence of site response, structural stiffness, and base fixity on seismic forces and deformations was not investigated in detail, as is necessary in the validation of future numerical tools.

The dynamic behavior of underground structures fixed to a stiff rock foundation differs greatly from structures founded on soil, since the lateral base movement is prevented. Past analytical and numerical studies (e.g., [2,5,15,19–21,27]) showed that underground structures with a fixed base experience larger dynamic earth pressures compared to structures that can translate laterally. In addition to the magnitude of thrust, the distribution of earth pressures along the wall height can have a great influence on seismic performance. However, there is no consensus among past studies on what shape the pressure profile takes for structures with a fixed base, as well as those that can translate laterally. Further, the influence of the frequency content of the base motion on the forces and deformations experienced by stiff-unyielding structures, whether fixed at the base or free to translate, has not been evaluated experimentally.

This paper focuses on the combined effects of far-field site response, base fixity and stiffness of the structure, and the frequency content of the base motion on the dynamic behavior of stiff-unyielding underground structures. Experimental data was obtained from four dynamic centrifuge tests conducted on small-scale model structures in dry, medium-dense Nevada sand with different structure stiffness, base fixity, and applied base motions. The model structures represented prototype reinforced concrete reservoirs having 11 to 12 m-high walls that are restrained against rotational movement at their roof and floor levels. A sequence of earthquake and sinusoidal motions with different frequencies was applied to the base of the container in flight. The performance of buried structures was evaluated in terms of accelerations, rotational and lateral displacements, seismic lateral earth pressures, and bending strains. The application of sinusoidal motions in particular allowed for a comprehensive study of the influence of loading frequency in relation to the fundamental frequency of the site and structure. The insight from these experiments is intended to guide the future modeling and design of an entire class of stiff-unyielding buried reservoir structures to withstand earthquake loading.

2. Experimental method

Dynamic tests of model reservoir structures were performed at 60g of centrifugal acceleration using the 5.5 m-radius, 400g-ton geotechnical centrifuge at the University of Colorado Boulder. The model specimens were prepared in a flexible shear beam (FSB) container developed by Ghayoomi et al. [9]. The four different centrifuge tests considered in this study are referred to as T-Flexible, T-BL (baseline), T-Stiff, and T-Fixed. T-Flexible, T-BL, and T-Stiff had the same test configuration shown in Fig. 1a, but different flexural rigidities of the structures, as detailed in Table 1. In T-Fixed, the same baseline structure as T-BL was used, which was bolted to the base of the FSB container to emulate a fixed-base condition, as shown in Fig. 1b.

Dry Nevada sand No. 120 (G_s=2.65; e_{min}=0.56; e_{max}=0.84; D_{50}=0.13 mm; C_u=1.67) was placed in the FSB container at a target relative density of D_r=60% (γ_{dry}=15.6 kN/m^3). The soil deposit was pluviated in layers using a hopper at a calibrated height to achieve the target relative density (D_r). However, the D_r of and geostatic stresses in sand near the structure walls were likely affected by the presence of the structure and silo effects, influencing the recorded earth pressures and bending strains on the walls to some extent. These effects in smaller models that are commonly used in centrifuge need to be considered when evaluating the experimental results and comparing them with future numerical simulations.

The experimentally-measured small-strain, fundamental frequency of the far-field soil column (f_{so}) was estimated in an average sense prior to applying any dynamic motions using the

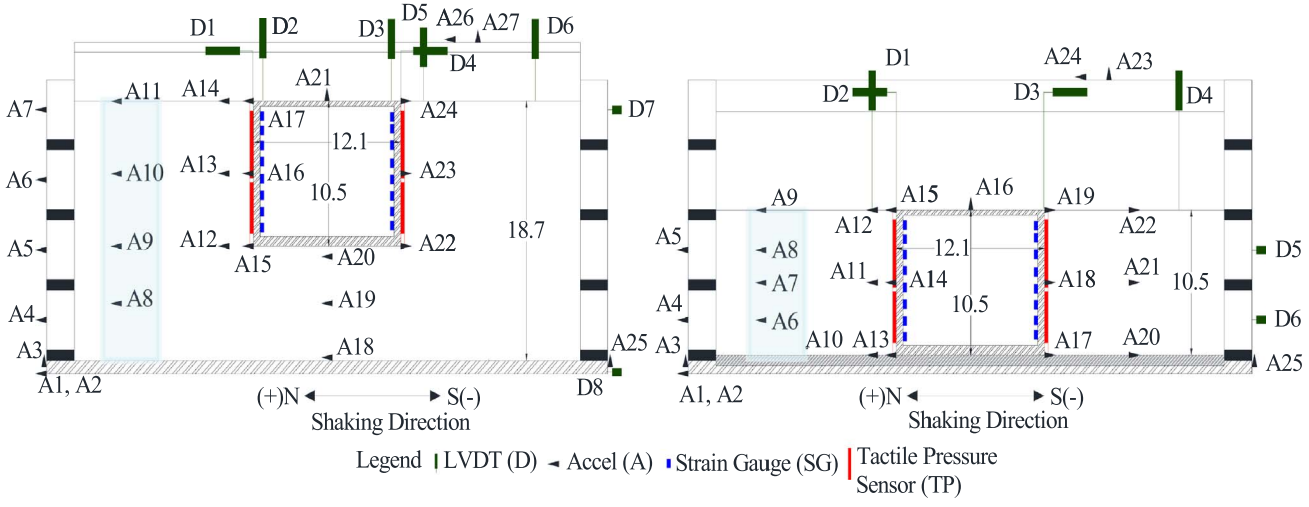

Fig. 1. Elevation views of centrifuge models in: (a) T-Flexible, T-BL, T-Stiff; and (b) T-Fixed. Notes: dimensions shown in prototype scale meters; highlighted region shows the far-field accelerometer array.

Table 1
Dimensions and properties of model structures used in centrifuge (prototype scale).

Test	Structure	Outer dimensions (m)	Thickness			Fundamental frequency (Hz)
			Base (m)	Roof (m)	Walls (m)	
T-BL, T-Fixed	Baseline	H= 10.5	0.69	0.37	0.56	4.0
T-Flexible	Flexible	W=12.1	0.50	0.28	0.28	2.0
T-Stiff	Stiff		1.46	1.12	1.13	9.9

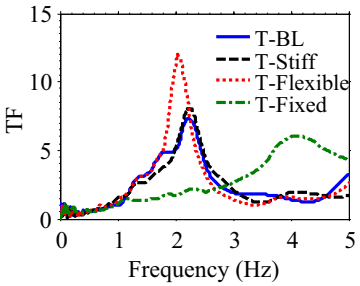

Fig. 2. Transfer Function (TF) of surface to base accelerations in the far-field under ambient vibrations, to obtain the small-strain fundamental frequency of far-field soil (f_{so}) in four tests (T-BL, T-Stiff, T-Flexible, T-Fixed).

Transfer Function (TF) of accelerations recorded at the soil surface to those at the container base under centrifuge ambient vibrations (prior to any shaking). The region treated as far-field in each test is highlighted in Fig. 1. The fundamental frequency of the far-field soil in T-Flexible, T-BL, and T-Stiff was compared with that in an initial free-field centrifuge experiment (with no structure present), and the results were consistent. This comparison indicated that the influence of structure and container boundaries on far-field soil f_{so} was minor. However, site response in the far-field may still have been affected by its proximity to container boundaries and the buried structure, particularly during stronger levels of shaking, which must be taken into account in the evaluation of experimental results and future numerical simulations.

The estimated f_{so} corresponding to the peak TF ranged from approximately 2.1 to 2.4 Hz in experiments T-Flexible, T-BL, and T-Stiff, and was approximately 4 Hz in T-Fixed, as shown in Fig. 2. The corresponding small-strain, average shear wave velocity of soil, $\bar{V}_s = 4 \cdot f_{so} \cdot H_{site}$, in the far-field ranged from approximately 157 to 180 m/s in T-Flexible, T-BL, and T-Stiff, and was approximately 166 m/s in T-Fixed.

The actual prototype reservoirs are complex structures with many columns and interior walls that support the weight of the roof slabs, walls resisting lateral shear forces, and other structural details, the three-dimensional (3D) response of which is difficult to simulate properly in a scaled centrifuge model. Accordingly, simplified, equivalent prototype two-dimensional (2D) box structures were identified and designed to match the mass, lateral stiffness, and natural frequency of the actual prototype reservoir structures (detailed by Hushmand et al. [11]). The model structures were constructed of four pieces of welded 1018 Carbon Steel (density = 7870 kg/m^3; Young's modulus = 2×10^8 kPa). The dimensions and natural frequencies of the structures used in different tests are summarized in Table 1. Teflon sheets were placed on both ends of the open structure to prevent the backfill sand from entering the structure, and were also placed on the sidewalls of the container to facilitate relative sliding, minimize friction, and simulate plane strain conditions.

Fig. 1 shows the number and location of sensors including accelerometers, linearly-variable differential transformers (LVDTs), strain gauges, and tactile pressure transducers that were used to measure the seismic response of the soil-structure system. Miniature piezoelectric accelerometers were used to measure accelerations in the soil, on the structure, and on the FSB container. The settlement of soil and structure and the lateral displacement of the structure, container frames, and container base were measured using LVDTs. Eight strain gauges were mounted along each wall of the structure in a half bridge configuration to measure bending strains. Two tactile pressure sensors (model number 9500, manufactured by Tekscan Inc.) were installed along the height of each wall of the structure perpendicular to the direction of shaking to measure static and seismic lateral earth pressures. The tactile sensors were equilibrated, conditioned, and statically and dynamically calibrated prior to use in centrifuge, following the procedure recommended by Dashti et al. [4], Gillis et al. [10], and El Ganainy et al. [7]. The acceleration, displacement, and strain data were recorded at a sampling frequency of 3000 samples per second (sps). The tactile sensors were attached to a different data acquisition system and had a sampling frequency of 4000 sps per sensel.

The motions were applied to the container base in flight using the servo-controlled, electro-hydraulic shake table [14]. The selected earthquake motions consisted of the following scaled horizontal records: Sylmar Converter Station of the 1994 Northridge Earthquake, the LGPC Station of the 1989 Loma Prieta Earthquake, and the Istanbul Station of the 1999 Izmit Earthquake in Turkey. The achieved base motions are referred to as Northridge-L (low intensity), Northridge-M (medium intensity), Northridge-H (high intensity), Izmit and Loma. The three Northridge motions used (L, M, and H) were scaled versions of the same motion, in order to evaluate the influence of ground motion intensity without major changes in its frequency content or duration. Fig. 3 presents the acceleration response spectra (5% damped) of the achieved (recorded) base motions in each of the four experiments. Table 2 summarizes the properties of base motions sequentially applied and recorded in each test in terms of peak ground acceleration (PGA), Arias Intensity (I_a), significant duration ($D_{5\text{-}95}$), and mean frequency (f_m). As expected, the largest difference in the properties of the achieved motions was observed during T-Fixed, in which the total weight of the model specimen was significantly different from the other tests.

The earthquake motions in each test were followed by a sequence of eight sinusoidal motions with similar amplitudes (primarily ranging from 0.3 to 0.5g) but different frequencies (0.33 Hz, 1 Hz, 2 Hz, 3 Hz, 4 Hz, 5 Hz, 6 Hz). Each sinusoidal motion had fifteen cycles. These motions enabled a comprehensive evaluation of the impact of the frequency of base motion on the response of the soil-structure system. As shown in Table 2, two earthquake motions were repeated after the sinusoidal motions to evaluate the response of the system after soil densification, followed by one final intense motion (Loma) and the highest frequency sinusoidal motion (6.7 Hz).

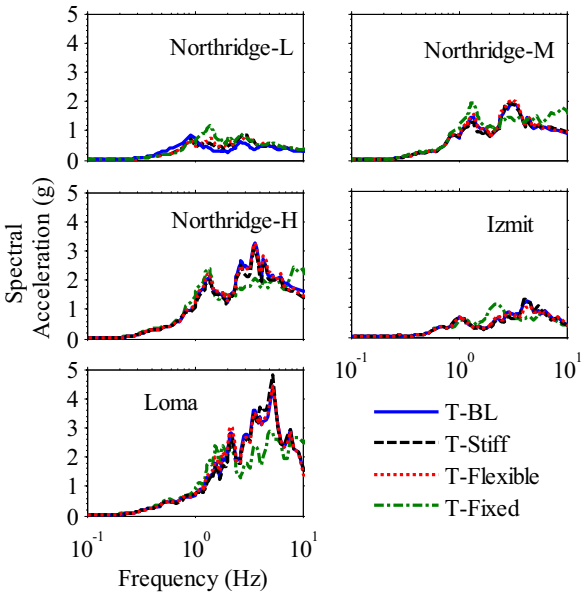

Fig. 3. Comparison of Northridge-L, Northridge-M, Northridge-H, Izmit, and Loma achieved base motion spectral accelerations (5%-damped) in four tests: T-BL, T-Stiff, T-Flexible, T-Fixed.

Table 2
Ground Motion Properties as measured in T-BL.

Shaking event	Input motion parameters			
	PGA (g)	I_a (m/s)	$D_{5\text{-}95}$ (s)	f_m (Hz)
Northridge-L1	0.26	1.3	21.6	0.9
Northridge-M	0.73	5.8	26.7	1.5
Northridge-H	1.26	12.9	26.7	1.7
Izmit-1	0.3	2.6	37.6	1.8
Sine 0.3	0.27	3.7	36.6	0.5
Sine 1	0.31	3.4	12.8	1.2
Sine 2	0.40	3.6	6.2	2.8
Sine 3	0.44	5.2	4.1	3.1
Sine 4	0.41	3.3	3.0	4.0
Sine 5	0.92	17.8	2.4	5.0
Sine 6	0.50	4.4	2.1	5.9
Northridge-L2	0.31	1.8	18.4	1.3
Izmit-2	0.32	2.8	39.1	1.8
Loma	1.05	15.0	12.8	2.3
Sine 6.7	0.50	4.6	15.1	6.9

3. Experimental results

3.1. Soil densification after subsequent motions

The application of successive motions changes the soil characteristics through shearing and densification, which consequently affects the accelerations, strains, and earth pressures experienced by the soil-structure system during shaking. Notable cumulative soil and structure settlements were observed after each successive ground motion in the centrifuge. Fig. 4 shows the cumulative settlement of the structure and soil in the near- and far-field during all the applied ground motions in one representative test (T-Flexible). The relative density of the far-field soil increased from approximately 60% to 73% during this test. The largest settlement occurred during the first three ground motions when the soil was at its loosest state. During T-Flexible, the lighter structure (as compared to the baseline and stiff structures) settled less than the adjacent soil and far-field. The settlement of the buried structure increased as its weight increased, as expected.

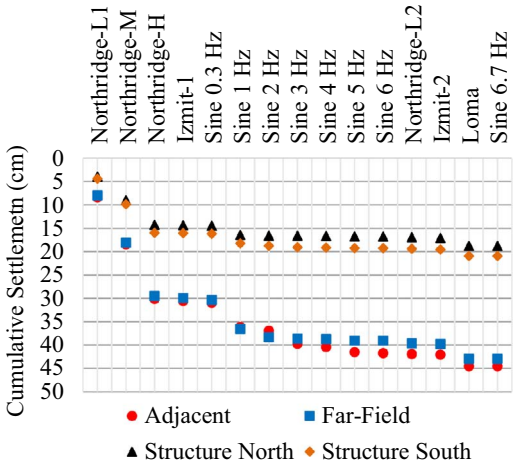

Fig. 4. Cumulative settlement of far-field soil, adjacent to structure, and structure during T-Flexible subject to different earthquake and sinusoidal motions.

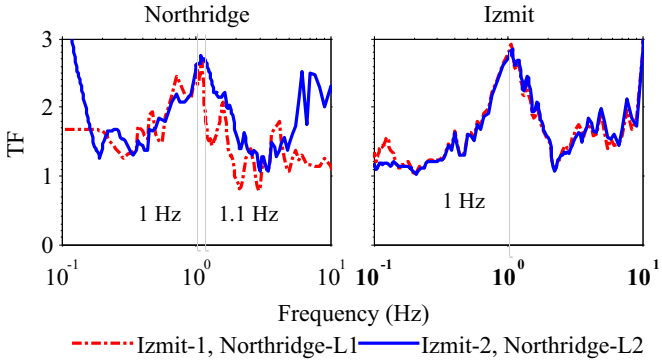

Fig. 5. Transfer functions of surface to base accelerations in the far-field in T-Flexible during the two sets of Izmit and Northridge-L motions.

The relative density of the granular backfill soil increased from 72% to 81% and from 60% to 75% in the centrifuge experiments conducted by Al Atik [1] and Stadler [23], respectively. However, the influence of soil densification and seismic history could not be evaluated in these experiments because the same motion was not repeated after multiple ground motions. The Northridge-L and Izmit ground motions in the presented experiments were repeated towards the end of the test (Table 2), which are referred to as Northridge-L2 and Izmit-2, in order to evaluate the influence of repetitive soil densification and shearing on the response of the soil-structure system.

The change in relative density (D_r) of the far-field soil was estimated to be ~12% between the Northridge-L1 and Northridge-L2 motions and 3% between the Izmit-1 and Izmit-2 motions. Fig. 5 compares the transfer function (TF) of accelerations at the surface to base in the far-field soil during Northridge-L1 or Izmit-1 with those during Northridge-L2 or Izmit-2, which were applied after several motions. No major change was observed in the effective, strain-dependent, fundamental frequency of the far-field soil (f_{so}') corresponding to the peak TF. In all the motions considered, f_{so}' of the far-field soil was estimated to range from approximately 0.92 to 1.3 Hz, which corresponds to an average, effective shear wave velocity ($\bar{V}_s'$) ranging from about 69 to 97 m/s.

Fig. 6 compares the amplification in peak ground accelerations (PGAs) along the far-field soil column from the base during the two sets of Northridge-L and Izmit motions. A de-amplification of PGA was prominent during the Northridge-L1 motion, with a looser soil column. After soil densification and subsequent shaking

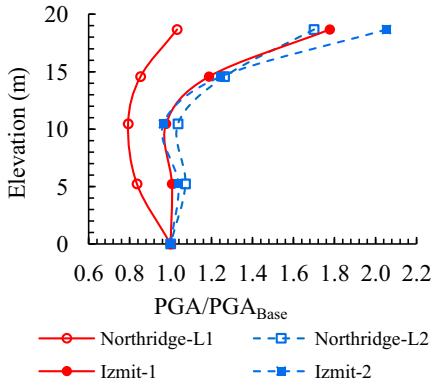

Fig. 6. PGA ratios versus depth in T-Flexible during the two sets of Izmit and Northridge-L motions.

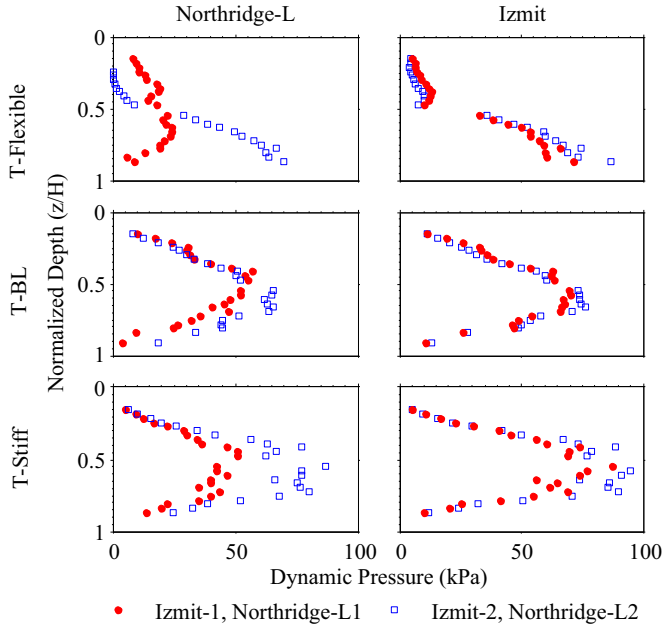

Fig. 7. Dynamic increment of earth pressures ($\Delta\sigma_E$) at time of maximum thrust during the two sets of Northridge-L and Izmit motions in T-Flexible, T-BL, and T-Stiff.

that changed the soil fabric, during Northridge-L2, amplification of PGA was prominent. The change in PGA amplification patterns was minimum from Izmit-1 to Izmit-2 motions, again because of minor soil densifications that occurred in between those two motions.

The dynamic increment of lateral earth pressures recorded on each structure during the two sets of Northridge-L and Izmit motions at the time corresponding to peak dynamic thrust is compared in Fig. 7. In general, the distribution and magnitude of seismic earth pressures were consistent during the two sets of motions, increasing slightly during the second set primarily due to densification. There was, however, one exception. As will be discussed in more detail in later sections, the distribution of seismic earth pressures was generally observed to change from linearly increasing with depth to a higher order polynomial as the structure's flexural stiffness was increased [11]. However, the flexible structure during T-Flexible, Northridge-L1 did not show the linearly increasing trend that was expected based on trends observed in the other tests and motions. This may be because of looser soil conditions near the wall face in this particular test leading to less contact between the backfill soil and the wall (or sensor) prior to

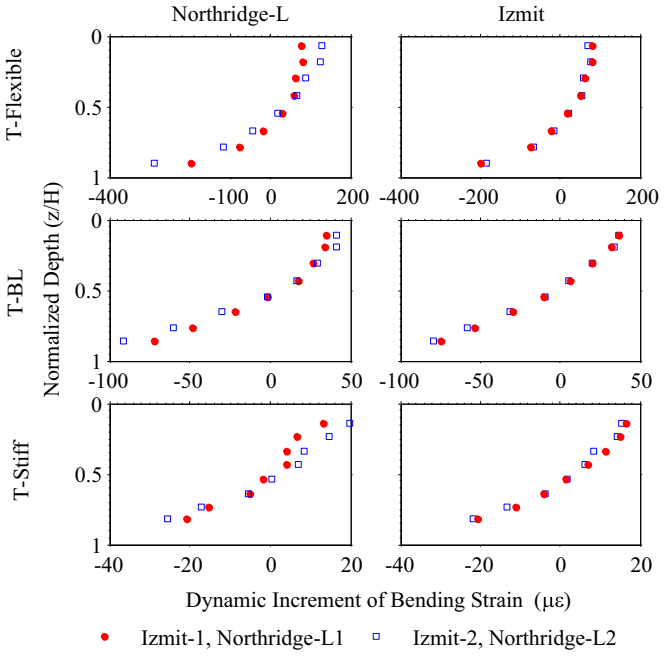

Fig. 8. The dynamic increment of bending strains ($\Delta\varepsilon_E$) at the time of maximum moment during the two sets of Northridge-L and Izmit motions in T-Flexible, T-BL, and T-Stiff.

the first motion. However, the distributions of earth pressures immediately following the first motion were more linear during T-Flexible. The influence of soil densification and fabric on the dynamic response of underground structures can also be evaluated in terms of dynamic strain profiles at the time of maximum moment (or strain), as shown in Fig. 8. The dynamic increment of strain was consistently slightly larger during the Northridge-L2 motion compared to L1. The change was negligible during the Izmit motions, as expected, with little soil densification between the two shakes.

3.2. Accelerations

The transfer functions of far-field soil surface to container base accelerations as well as structure roof to container base accelerations for the different structures and earthquake motions are shown in Fig. 9. The highlighted area shows the approximate range of effective, strain-dependent, fundamental frequencies (f_{so}') of the far-field soil and the soil-structure system. The f_{so}' ranged from approximately 0.92 to 1.3 Hz during T-BL, T-Stiff, and T-Flexible for both the far-field soil column and the soil-structure system (in an average sense). The estimated f_{so}' in T-Fixed ranged from approximately 2.2 to 3.5 Hz. The fundamental frequency of the buried structure-soil system was primarily controlled by the response of the far-field soil rather than the fixed-base fundamental frequency of the isolated structure.

The amplification or de-amplification of peak accelerations (PGAs) from the base of the container to the soil surface in the far-field or to the structure roof in T-BL, T-Flexible, T-Stiff, and T-Fixed during the different earthquake motions are shown in Fig. 10. The base motion accelerations were amplified at the lower levels of shaking ($PGA_{base} \sim 0.3g$) and started to de-amplify at higher levels of shaking ($PGA_{base} > 0.6g$) as expected, due to additional soil nonlinearity and damping. Larger accelerations were recorded on the structure in T-Fixed compared to the other experiments that allowed transient rocking, settlement, and damping of seismic energy. The accelerations on the fixed-based buried structure were

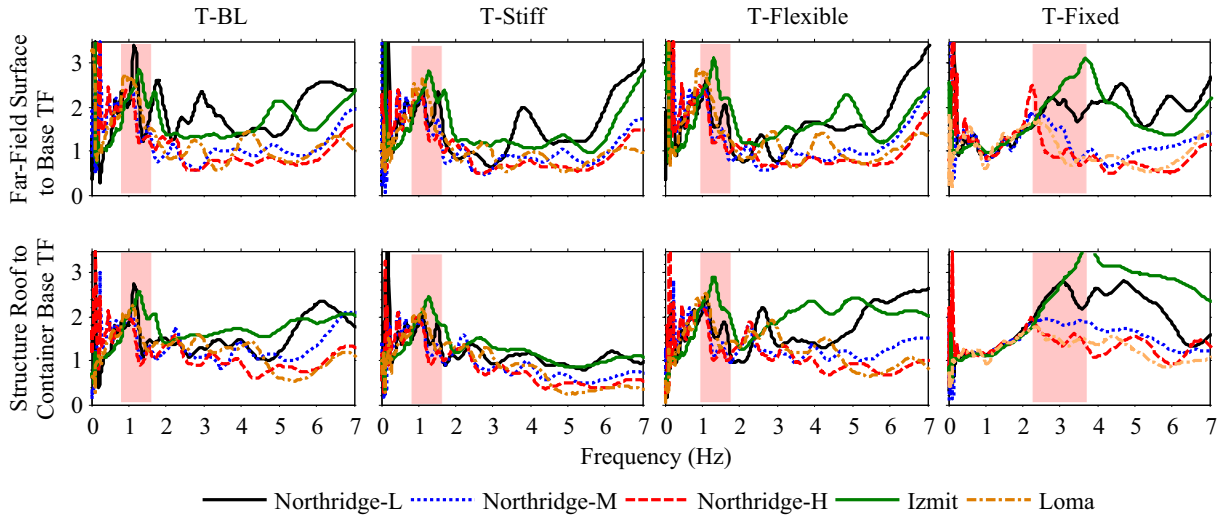

Fig. 9. Transfer functions of far-field surface to container base as well as structure roof to container base accelerations during different experiments and earthquake motions. The highlighted area marks the range of effective, strain-dependent, fundamental frequencies (f_{so}') near the peak values of TF.

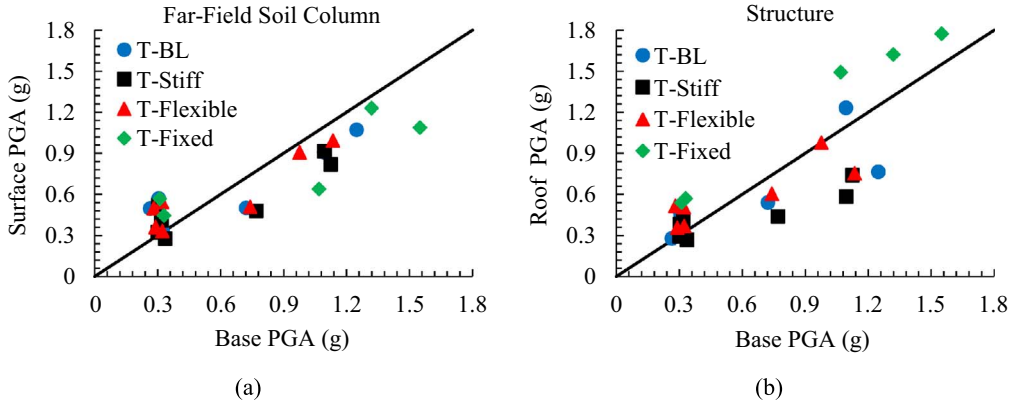

Fig. 10. Amplification or de-amplification of peak ground acceleration (PGA) from the container base to: (a) the far-field soil surface; and (b) the roof of four structures (BL, Stiff, Flexible, Fixed) during different earthquake motions.

amplified at stronger levels of shaking, more similar to what is expected for an aboveground structure. The buried structures resting on soil, however, generally experienced de-amplification of accelerations at stronger levels of shaking similar to the surrounding soil column.

The spectral ratios of acceleration at the top of the structure to those in the far-field soil in each test during different earthquake motions are compared in Fig. 11. Overall, the acceleration response of the structure was amplified compared to the far-field in frequencies ranging from about 2 to 5 Hz for all motions and structures. Increasing the flexibility of the structure often slightly increased its acceleration amplification with respect to the far-field due to a greater deflection near the roof. The spectral ratio of the structure in T-Fixed was greater compared to the other three tests, because of the kinematic constraint imposed at the base of the structure, amplifying its acceleration more pronouncedly relative to the far-field soil.

3.3. Structural tilt

The time histories and Fourier Amplitude Spectra of tilt measured on the three structures with a flexible base (i.e., T-Flexible, T-BL, and T-Stiff) during three representative shaking events (Northridge-L, Northridge-M, Northridge-H) are compared in

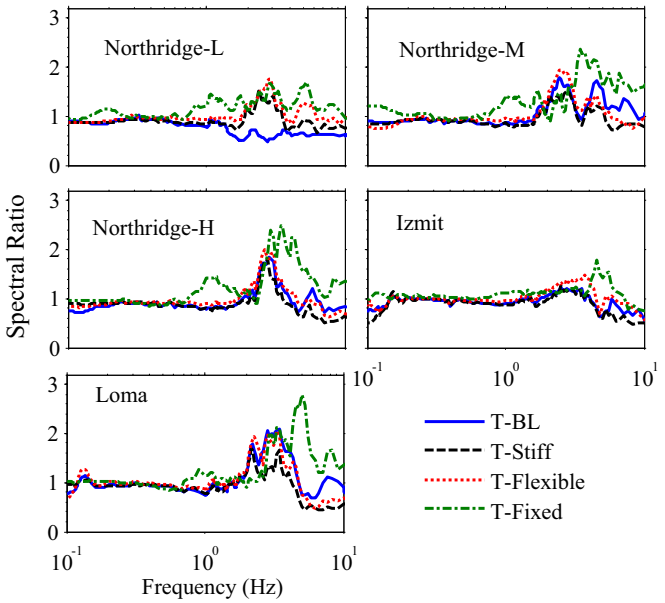

Fig. 11. Spectral ratio (5% damped) of structure to far-field accelerations at the elevation corresponding to the roof of the structure in four tests (T-BL, Flexible, Stiff, Fixed) during different earthquake motions.

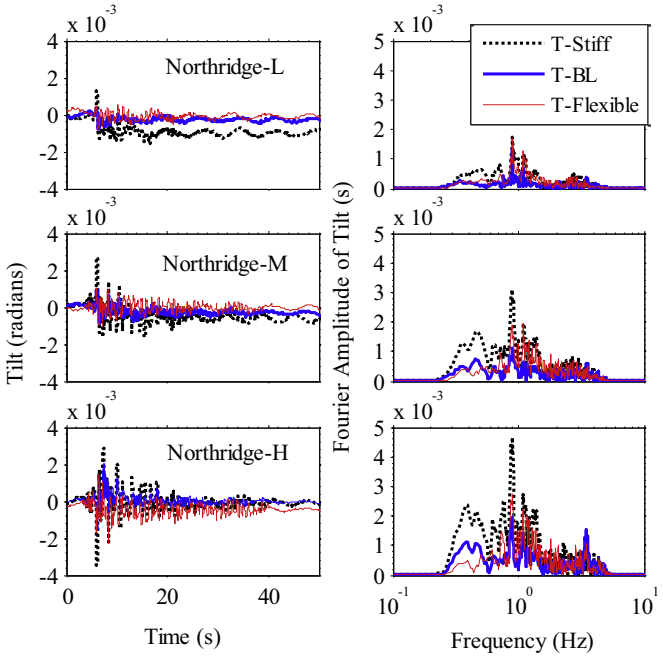

Fig. 12. Time histories and Fourier Amplitude Spectra of structural tilt in T-Flexible, T-BL, and T-Stiff during the Northridge motions.

Fig. 12. The tilt of the structure was obtained by dividing the difference in the recordings of vertical LVDTs on the edges of the structure roof (D2 and D3) by the width of the structure. The degree of structural tilt or rocking was observed to amplify as the shaking intensity increased, as expected. Increasing the structural mass (i.e., from Flexible to BL to Stiff) consistently increased its transient and residual tilt during all shaking events, which was expected due to a greater inertia and seismic moment that would amplify the rocking response of the buried structure. The frequency content of the structural tilt was observed to be similar among the different tests, however. The primary frequency content of structural tilt was observed at approximately 1 Hz, which was near the mean frequency of the base motion (f_m) as well as the site's effective fundamental frequency (f_{so}') during these experiments and motions, regardless of variations in the fundamental frequency of the isolated structure. The rocking response of the structure was expected to influence the distribution and amplitude of lateral earth pressures, which is discussed in more detail in the following section.

3.4. Seismic earth pressures

The dynamic increment of pressure ($\Delta\sigma_E$) was obtained directly from tactile pressure sensors by subtracting the pre-shake static pressure from the total value (static and dynamic) at a given depth and time. It must be noted that friction was minimized on

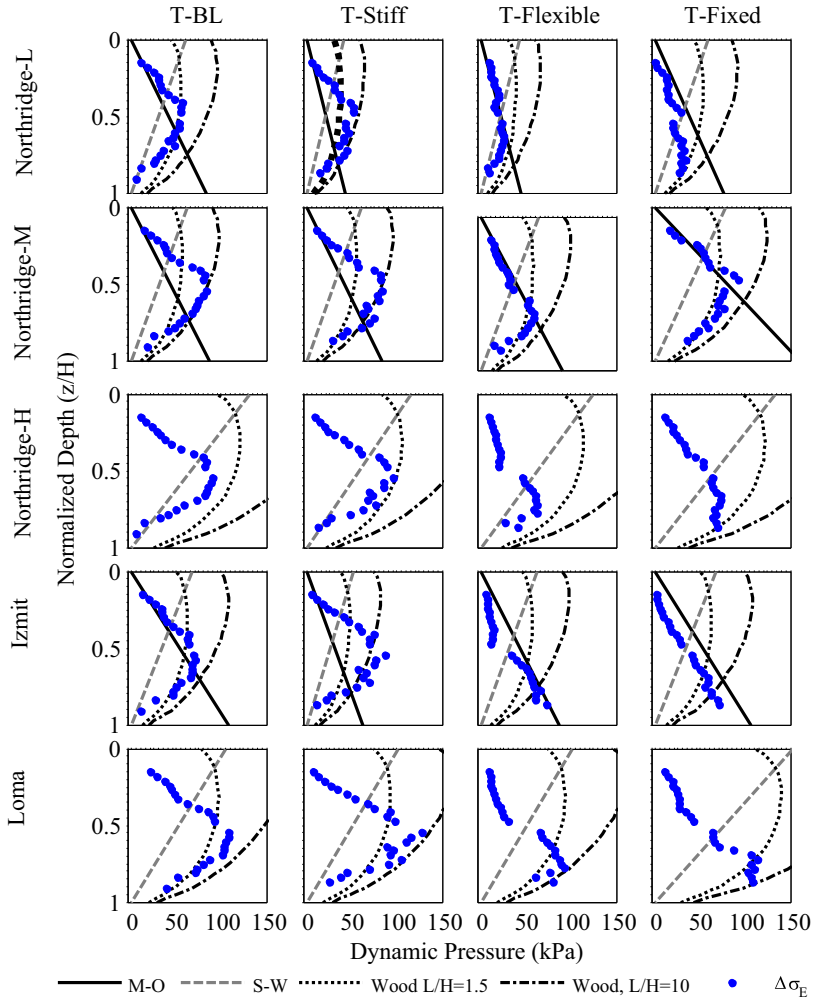

Fig. 13. Dynamic increment of earth pressure ($\Delta\sigma_E$) at the time of maximum thrust during four experiments (T-BL, T-Stiff, T-Flexible, T-Fixed) compared to the M-O, S-W, and Wood analytical methods. Measurements provided along the height of the wall (z=depth along the wall, H=height of the wall).

the face of the tactile sensors by using Teflon sheets (as detailed by Gillis et al. [10] and Hushmand et al. [11]) to reduce shear stresses on the sensors and improve their reliability in measuring normal pressure. However, this interface condition is different from what is typically expected on the walls of buried, reinforced concrete, reservoir structures. This difference may influence the distribution of lateral earth pressures and bending strains.

Dynamic thrust acting on each structure during a given motion was estimated by numerically integrating the dynamic distribution of earth pressures at each instance of time. The presented thrust time histories were subject to a band-pass, fifth-order, acausal, Butterworth filter with corner frequencies of 0.1–15 Hz, to remove low and high frequency noise that was sometimes present in the tactile sensor records and could affect the estimated time of peak dynamic thrust. As a result of filtering, however, any permanent change in lateral earth pressures (which could be real) was removed from the data.

The values of $\Delta\sigma_E$ at the time of maximum dynamic thrust in four tests (T-BL, T-Stiff, T-Flexible, T-Fixed) during different earthquake motions are compared in Fig. 13. The three centrifuge experiments with different structures (T-BL, T-Stiff, and T-Flexible) were all repeated once to ensure repeatability of the results, and the measurements were consistent. A few of the most common analytical methods used to calculate dynamic earth pressures on retaining structures are also plotted for comparison: Mononobe-Okabe (M-O) and Seed-Whitman (S-W) assuming yielding (or active) conditions, and Wood, assuming rigid-unyielding conditions.

To obtain analytical solutions of seismic earth pressures during each motion, 100% of the PGA recorded in the far-field soil surface (i.e., using sensor A9 in T-Fixed and A11 in the other tests) was employed for all procedures. The M-O method provided indeterminate values of earth pressure at PGA values greater than 0.7g for a soil friction angle of 35°. Therefore, the M-O solution is not presented in Fig. 13 during the Northridge-H and Loma motions. The S-W procedure uses an inverted triangle dynamic earth pressure profile, as shown in Fig. 13. Wood's simplified procedure was computed based on an L/H ratio of 1.5 corresponding to the centrifuge tests, but was also computed based on a larger L/H of 10 for comparison, where L is the lateral extent of the backfill soil and H is the wall height. Wood's procedure does not take into account the increase in soil shear modulus with depth and therefore predicted large $\Delta\sigma_E$ values near the top of the wall compared to those observed.

The distribution of $\Delta\sigma_E$ in experiments T-BL, T-Stiff, and T-Flexible depended greatly on the flexural rigidity of the structure, as also confirmed by other studies [8,13,20,26]. Increasing the flexibility of the structure (e.g., T-Flexible compared to T-BL and T-Stiff) tended in general to change the distribution of $\Delta\sigma_E$ from a

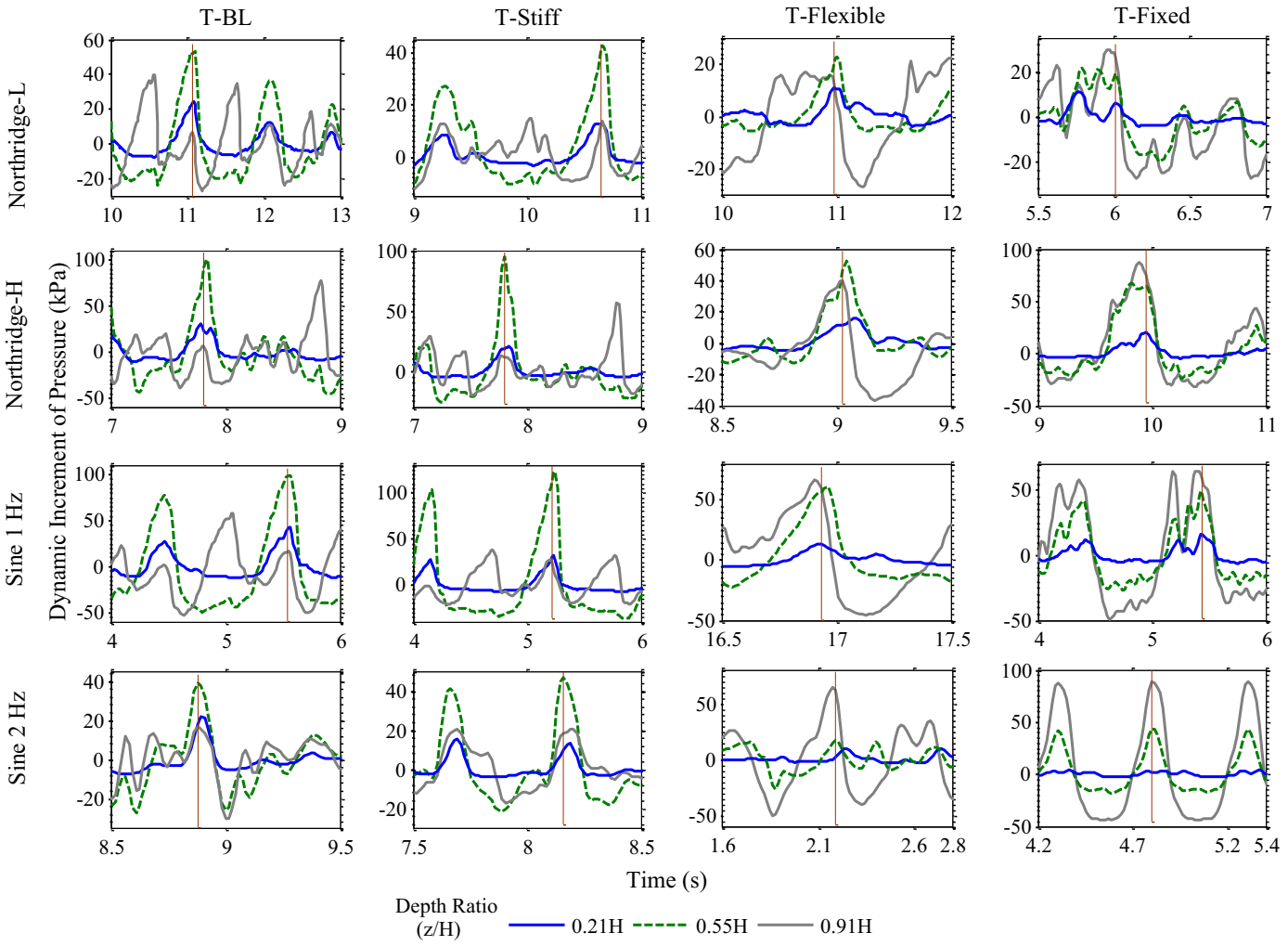

Fig. 14. Dynamic pressure time histories at the top, middle, and bottom of the structure wall during a few representative (Northridge-L, Northridge-H, Sine 1 Hz, Sine 2 Hz) ground motions. The vertical line identifies the time of maximum dynamic thrust on the wall.

parabola to an approximately triangular distribution mainly increasing with depth. Fixing the base of the structure in T-Fixed, on the other hand, generally increased $\Delta\sigma_E$ near the base of the BL structure compared to T-BL (particularly after the first motions when a better contact between sand grains and tactile sensors was established), likely because of the greater inertial demand applied to the base of the structure without the ability to settle or rock with respect to the surrounding soil. This observation is consistent with the numerical results presented by Psarropoulos [20]. Importantly, as shown in Fig. 13, none of analytical solutions could sufficiently capture the distribution and magnitude of seismic earth pressures experienced on this class of underground structures in a consistent manner.

Time histories of dynamic lateral earth pressure at the top, middle, and bottom of the structures during four representative earthquake and sinusoidal motions (e.g., Northridge-L, Northridge-H, Sine 1 Hz, Sine 2 Hz) in each test are compared in Fig. 14. In general, the $\Delta\sigma_E$ time histories were observed to be in phase along the height of the wall for the stiffer structures (T-BL, T-Stiff, and T-Fixed). The more flexible structure in T-Flexible, however, experienced $\Delta\sigma_E$ time histories that were slightly out of phase. The pressures peaked near the bottom before the middle and top. This was due to larger wall deflections increasing from the base to roof of the flexible structure as shown in Fig. 8, which contributed to the overall reduction of dynamic earth pressures and forces as compared to the other cases.

The short-term Fourier transform (STFT) of accelerations recorded on the container base and mid-depth of the structure wall are compared to those of dynamic thrust during the Northridge-L motion in each of the four tests in Fig. 15. The base acceleration contained a significant content near 1 Hz in all experiments during Northridge-L, particularly in the early part of the record. Similarly, the accelerations recorded at the mid-depth of the structure and the dynamic thrust in T-Flexible, BL, and Stiff showed maximum content near 1–1.5 Hz, which coincided with the effective natural frequency of the site (f_{so}') in those tests.

In T-Fixed, the f_{so}' of the shallower soil deposit ranged from approximately 2.2 to 3.5 Hz during different motions, corresponding to the peak of the surface to base transfer functions in the far-field. An important frequency content was observed in the structure's acceleration and dynamic thrust near 2–3 Hz in this test, but this frequency range was not dominant. The base of the fixed structure experienced the same motion as the base of the container, with no influence from site response. However, along the height of the wall, the structure's acceleration was influenced slightly by site response, as also shown previously in Figs. 9 and 11. Hence, the Fourier amplitude of accelerations at the mid-depth of the wall showed amplification compared to the base near f_{so}' of approximately 2–3 Hz in T-Fixed. The dynamic thrust during this test also had content near 2–3 Hz corresponding to f_{so}', but its primary content was observed near 1 Hz over an extended period of time, corresponding to the mean frequency (f_m) of the base motion. The sinusoidal motions (with a narrow frequency content) allowed an easier evaluation of the impact of f_{so}' alone on the response of the structure.

The profiles of $\Delta\sigma_E$ at the time of maximum thrust are compared in Fig. 16 for four tests (T-BL, T-Stiff, T-Flexible, T-Fixed) during sinusoidal motions that were achieved with roughly similar amplitudes (mostly ranging from about 0.3 to 0.5g) but frequencies that varied between 0.33 Hz and 6.7 Hz. The shape of the $\Delta\sigma_E$ profile did not appear to have a significant dependence on the excitation frequency, and was primarily affected by the relative stiffness of the structure and base fixity, as observed previously during broadband earthquake motions. The largest dynamic pressures for all tests occurred when the base excitation frequency of the sinusoidal motion approached the far-field soil f_{so}'. In tests T-BL, T-Stiff, and T-Flexible the largest pressures were recorded at an excitation frequency of 1 Hz, near the far-field f_{so}' in those tests. The largest dynamic pressures in T-Fixed were recorded at an excitation frequency near 2–3 Hz, again near its far-field f_{so}'. At higher or lower frequencies, the dynamic increment of pressure reduced greatly compared to the resonance condition.

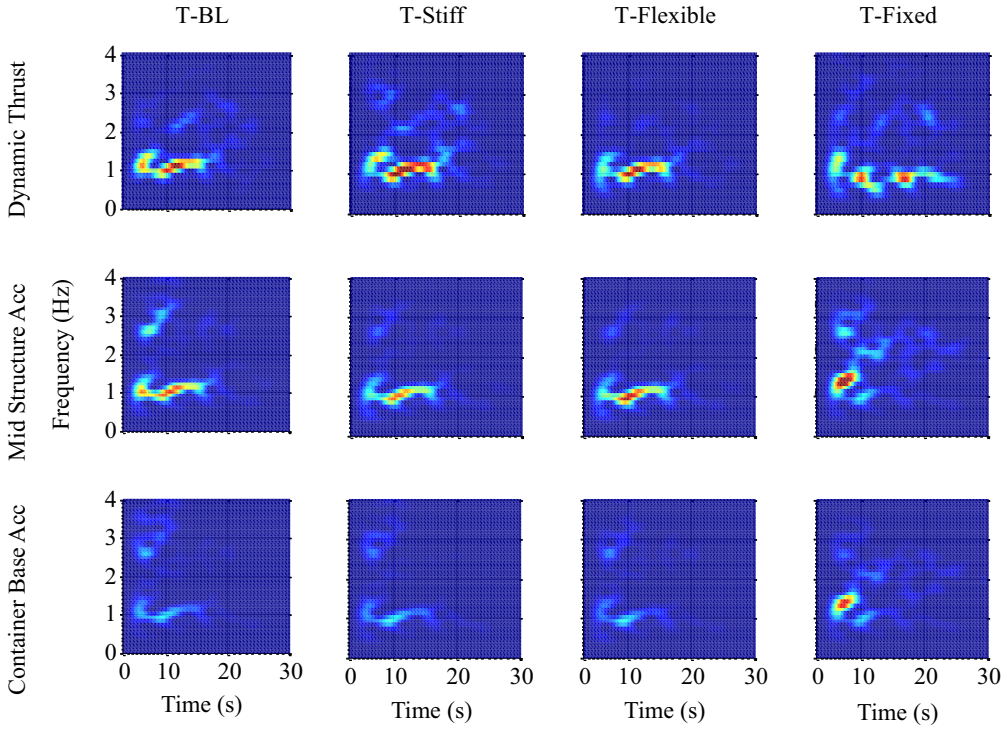

Fig. 15. Short-term Fourier transform (STFT) of container base acceleration, mid-depth structural wall acceleration, and dynamic thrust recorded on the structure in T-Flexible, T-BL, T-Stiff, and T-Fixed during the Northridge-L motion. Red color denotes high amplitude, and blue indicates low amplitude.

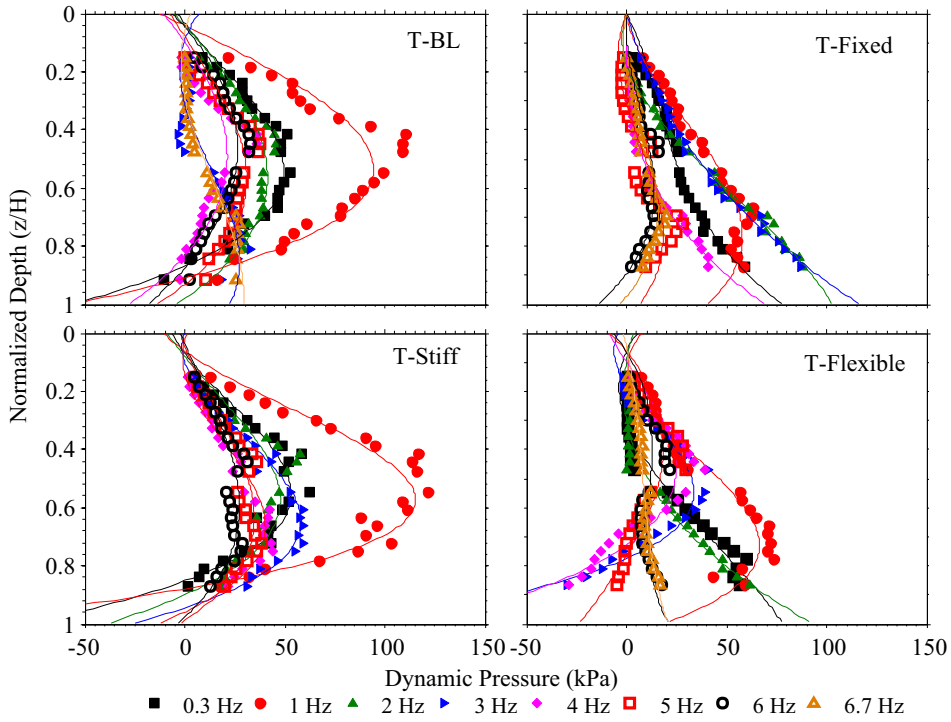

Fig. 16. Dynamic increment of pressure ($\Delta\sigma_E$) at time of maximum thrust during four tests and eight sinusoidal motions with different frequencies along the height of the wall (z = depth, H = height of the wall, data points = tactile sensor recordings, solid lines = best fit curves). Note: pressure recordings were not obtained in T-Stiff during Sine-6.7 Hz.

3.5. Dynamic strains

Bending strains were measured with strain gauges installed on the inside walls of the structures during and after each ground motion. The largest dynamic bending strains ($\Delta\varepsilon_E$) were often recorded near the base of the structure. The dynamic bending strain ($\Delta\varepsilon_E$) profiles are shown in Figs. 17 and 18 at the times of maximum strain (or maximum moment) during different earthquake and sinusoidal motions, respectively. Tensile surface bending strain (i.e., outward wall curvature) is shown as positive in these figures. Dynamic bending strains may be used to also evaluate the magnitude and distribution of dynamic bending moments on the walls. As expected, bending strains decreased when increasing the flexural stiffness of the structure. Additionally, as shown in Fig. 19, fixing the base of the structure to the container in T-Fixed generally amplified dynamic strains compared to T-BL, particularly at the base. Similar to dynamic earth pressures in Fig. 16, dynamic strains in Fig. 18 were observed to peak when the excitation frequency approached the effective fundamental frequency of the far-field site in the corresponding test (f_{so}' near 1 Hz in T-BL, T-Stiff, T-Flexible; and f_{so}' near 2–3 Hz in T-Fixed).

4. Concluding remarks

A series of dynamic centrifuge tests were conducted to study 10.5 m-high box structures with varying flexural rigidities and fixity conditions, buried in medium-dense, dry sand undergoing 1D horizontal shaking. All structures had their roofs at the ground surface. The base motions consisted of various earthquake motions with PGAs ranging from 0.26 to 1.39g and sinusoidal motions with similar amplitudes (mostly ranging from about 0.3 to 0.5g), but frequencies ranging from 0.33 Hz to 6.7 Hz. The results of this experimental study indicate the following trends:

1. Soil densification (D_r increase from approximately 60% to 72%) and shearing after multiple motions resulted in greater PGA amplifications along the far-field soil column, greater static and seismic lateral earth pressures, and slightly greater dynamic bending strains along the height of the wall, but did not noticeably influence the effective fundamental frequency of the site (f_{so}').
2. The seismic response of the buried structure fixed at the base was noticeably different from the structures resting on soil with the ability to settle or rock. The structure to far-field acceleration spectral ratios and dynamic earth pressures were greater on the fixed structure compared to others.
3. The seismic performance of the buried structure in terms of tilt, acceleration, dynamic thrust, and dynamic bending strains was influenced greatly by the frequency content of the base motion as well as far-field site response. During the sinusoidal motions (with a narrower frequency band compared to earthquake motions), the dynamic earth pressures and bending strains always peaked when the excitation frequency approached far-field soil's f_{so}', regardless of the fundamental frequency of the structure or base fixity. This observation points to the critical importance of site response and resonance on the performance of buried reservoir structures.
4. The magnitude of seismic thrust increased and the distribution of seismic earth pressures changed from approximately triangular to parabolic with increasing structural stiffness. The shape or distribution of dynamic earth pressures was shown as relatively independent of the excitation frequency and mainly dependent on the structure's relative stiffness and base fixity.
5. None of the analytical solutions could consistently capture the distribution and magnitude of seismic earth pressures for the range of flexural stiffness, boundary conditions, and ground motion intensities often used in the design of underground reservoir structures.

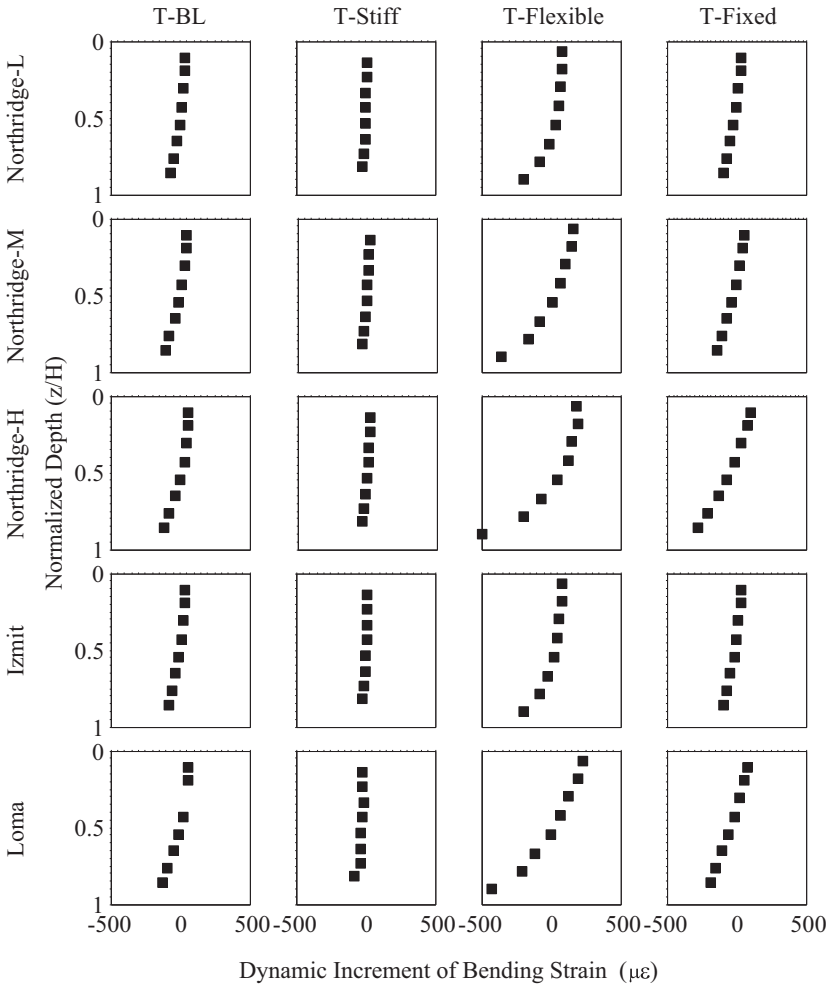

Fig. 17. Dynamic increment of bending strain ($\Delta\varepsilon_E$) at the time of maximum strain during four experiments (T-BL, T-Stiff, T-Flexible, T-Fixed) and different earthquake motions.

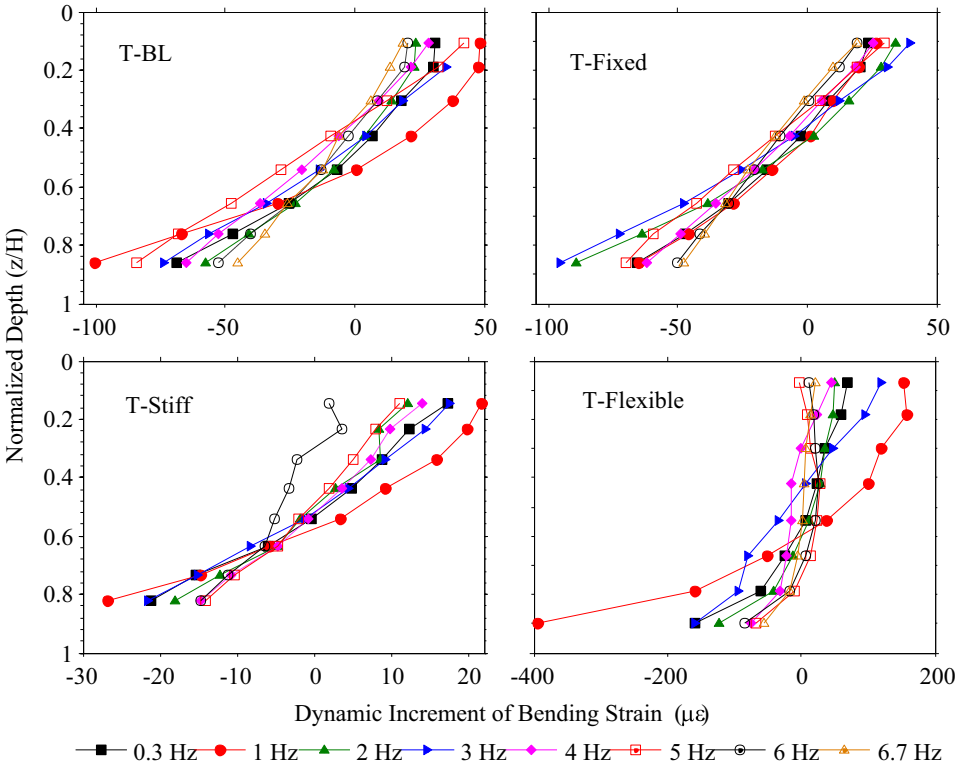

Fig. 18. The dynamic increment of bending strains ($\Delta\varepsilon_E$) at the time of maximum strain during four tests (T-BL, T-Stiff, T-Flexible, T-Fixed) and eight sinusoidal motions with different frequencies.

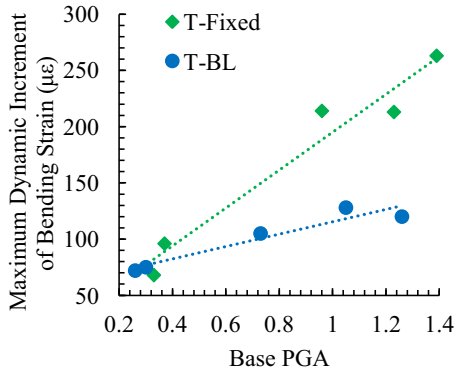

Fig. 19. Maximum dynamic increment of bending strain at the base of structure versus base motion PGA during T-Fixed and T-BL.

The analytical procedures commonly employed to evaluate the seismic response of underground structures do not adequately consider the range of soil properties, flexural stiffness, kinematic constrains, and ground motion characteristics for which critical underground reservoir structures must be designed. Advanced numerical methods may also assume simplistic soil properties, boundary conditions, or seismic loading that may not be applicable to realistic conditions and may at times lead to misleading conclusions. The experimental results presented in this paper are intended to help systematically evaluate the influence of soil densification, flexural stiffness, base fixity, site response, and ground motion characteristics on the seismic performance of stiff-unyielding buried structures. Parallel nonlinear numerical simulations validated using the centrifuge results but considering other variations than those permitted in the experiments are necessary and underway. These simulations are needed before generalized recommendations may be provided.

Acknowledgments

The authors would like to thank the Los Angeles Department of Water and Power (LADWP) and the Department of Civil, Environmental, and Architectural Engineering at the University of Colorado Boulder for financial support of this research. We would also like to thank Drs. Min Zhang, Jianping Hu, Yangsoo Lee, and Majid Ghayoomi for their support in the planning, design, execution, and interpretation of the centrifuge experiments.

References

[1] Al Atik L, Sitar N. Seismic earth pressures on cantilever retaining structures. J Geotech Geoenviron Eng 2010;136(10):1324–33.
[2] Brandenberg SJ, Mylonakis G, Stewart JP. Kinematic framework for evaluating seismic earth pressures on retaining walls. J Geotech Geoenviron Eng 2015. http://dx.doi.org/10.1061/(ASCE)GT.1943-5606.0001312 (04015031).
[3] Cilingir U, Madabhushi SG. Effect of depth on the seismic response of square tunnels. Soils Found 2011;51(3):449–57.
[4] Dashti S, Gillis K, Ghayoomi M, Hashash Y. Sensing of lateral seismic earth pressures in geotechnical centrifuge modeling. In: Proceedings of 15th world conference on earthquake engineering. Lisbon, Portugal; 2012.
[5] Davis CA. Lateral seismic pressures for design of rigid underground lifeline structures. In: Proceedings of the 6th U.S. conference on lifeline earthquake engineering. ASCE; 2003. p. 1001–10.
[6] Dewoolkar MM, Ko H, Pak RYS. Seismic behavior of cantilever retaining walls with liquefiable backfills. J Geotech Geoenviron Eng 2001;127:424–35.
[7] El Ganainy H, Tessari A, Abdoun T, Sasanakul I. Tactile pressure sensors in centrifuge testing. ASTM Geotech Test J 2014;37(1):151–63.
[8] Gazetas G, Psarropoulos PN, Anastasopoulos I, Gerolymos N. Seismic behavior of flexible retaining systems subjected to short-duration moderately strong excitation. Soil Dyn Earthq Eng 2004;24(7):537–50.
[9] Ghayoomi M, Dashti S, McCartney JS. Performance of a transparent flexible shear beam container for geotechnical centrifuge modeling of dynamic problems. Soil Dyn Earthq Eng 2013;53:230–9.
[10] Gillis K, Dashti S, Hashash Y. Dynamic calibration of tactile sensors for measurement of soil pressures in centrifuge. ASTM Geotech Test J 2015;38(3):261–74.
[11] Hushmand A, Dashti S, Davis C, Hushmand B, Zhang M, Ghayoomi M, McCartney JS, Lee Y, Hu J. Seismic performance of underground reservoir structures: insight from centrifuge modeling on the influence of structure stiffness. J Geotech Geoenviron Eng ASCE 2016. http://dx.doi.org/10.1061/(ASCE)GT.1943-5606.0001477.
[12] Hushmand A, Dashti S, Davis C, Hushmand B, McCartney J, Hu J, Lee Y. Seismic performance of underground reservoir structures: insight from centrifuge modeling on the influence of backfill soil type and geometry. J Geotech Geoenviron Eng ASCE 2016. http://dx.doi.org/10.1061/(ASCE)GT.1943-5606.000154404016058.
[13] Jung C, Bobet A. Seismic earth pressures behind retaining walls: effects of rigid-body motions. In: Proceedings of Geotechnical Earthquake Engineering and Soil Dynamics IV. ASCE, Reston, VA; 2008. p. 1-11.
[14] Ketcham SA, Ko HY, Sture S. Performance of an earthquake motion simulator for a small geotechnical centrifuge. In: Ko HY, McLean FG, editors. Centrifuge 91. Balkema, Rotterdam, The Netherlands; 1991. p. 361–8.
[15] Li X. Dynamic analysis of rigid walls considering flexible foundation. J Geotech Geoenviron Eng 1999;125(9):803–6.
[16] Mikola R. Seismic earth pressures on retaining structures and basement walls in cohesionless soils(Ph.D. thesis).Berkeley, CA: University Of California; 2012.
[17] Mononobe N, Matsuo, M. On the determination of earth pressures during earthquakes. In: Proceedings of world engineering congress, vol. 9; 1929. p. 179–87.
[18] Okabe S. General theory of earth pressure. J Jpn Soc Civil Eng 1926;12:1.
[19] Ostadan F. Seismic soil pressure for building walls: an updated approach. Soil Dyn Earthq Eng 2005;25(7):785–93.
[20] Psarropoulos PN, Klonaris G, Gazetas G. Seismic earth pressures on rigid and flexible retaining walls. Int J Soil Dyn Earthq Eng 2005;25:795–809.
[21] Richards R, Huang C, Fishman KL. Seismic earth pressure on retaining structures. J Geotech Geoenviron Eng 1999;125:771–8.
[22] Seed HB, Whitman RV. Design of earth retaining structures for dynamic loads. In: Proceedings of ASCE specialty conference, lateral stresses in the ground and design of earth retaining structures. Cornell Univ., Ithaca, New York; 1970. p. 103–47.
[23] Stadler AT. Dynamic centrifuge testing of cantilever retaining walls.Boulder, Co: Univ. of Colorado at Boulder; 1996.
[24] Tsinidis G, Pitilakis K, Madabhushi G, Heron C. Dynamic response of flexible square tunnels: centrifuge testing and validation of existing design methodologies. Geo-Technique 2015;65(5):401–17.
[25] Veletsos AS, Younan AH. Dynamic modeling and response of soil-wall systems. J Geol Eng 1994;120:2155–79.
[26] Veletsos AS, Younan AH. Dynamic response of cantilever retaining walls. J Geotech Geoenviron Eng 1997;123(2):161–72.
[27] Wood JH. Earthquake induced soil pressures on structures (Ph.D. thesis).Pasadena, CA: California Institute of Technology; 1973.